PHILOSOPHICAL MAGAZINE A, 2000, VOL. 80, NO. 12, 2841–2854

The mechanics of slip transition at intermediate temperatures in ⟨001⟩-oriented NiAl single crystals I. Experimental observations of the decomposition of $a\langle 111\rangle$ dislocations in Ni–44 at.% Al

R. SRINIVASAN†¶, J. BROWN‡, M. S. DAW‡§, R. D. NOEBE‖ and M. J. MILLS†

† Department of Materials Science and Engineering, The Ohio State University, Columbus, Ohio 43210, USA
‡ Department of Physics and Astronomy, Clemson University, Clemson, South Carolina 29634-1911, USA
§ Computational Materials Group, Motorola, 3501 Ed Bluestein Boulevard, MD K10, Austin, Texas 78721, USA
‖ Glenn Research Center, National Aeronautics and Space Administration, Cleveland, Ohio 44135, USA

[*Received 25 October 1999 and accepted 7 February 2000*]

ABSTRACT

Ni–44 at.% Al single crystals were studied after compressive deformation along the hard orientation between 700 and 825 K. In order to understand the mechanism of the slip transition occurring at intermediate temperatures, compression was performed at various strain rates and to various strain levels. Local decomposition of $a\langle 111\rangle$ dislocations was observed between 750 and 800 K. At 800 K (the slip transition temperature), complete decomposition occurs into $a\langle 101\rangle$ and $a\langle 010\rangle$ dislocations. Several unique features are associated with this decomposition event, such as the preference for near-edge line directions (for the $a\langle 111\rangle$ dislocations), significant strain softening between 800 and 900 K, and the effect of thermal activation in determining the extent of the actual decomposition event.

§ 1. INTRODUCTION

NiAl has been the subject of extensive research because of its potential to replace Ni-based superalloys in high-temperature structural applications in the aerospace industry. It has several desirable properties, including a low density (two thirds that of a superalloy), high melting point and excellent oxidation and corrosion resistances. In addition, it has excellent thermal conductivity which can reduce the 'hot-spot' temperature of turbine blades and vanes by 50 K, but NiAl also suffers from lack of strength at high temperatures, and poor ductility at low temperatures. Recent progress has been achieved, however, in both of these areas (Darolia *et al.* 1992, Noebe and Garg 1995, Levit *et al.* 1996).

The usual mode of deformation in both single-crystal and polycrystalline NiAl is through motion of $a\langle 010\rangle$ dislocations at all temperatures. However, on stressing

¶ Email: srini@mse.eng.ohio.state.edu

Philosophical Magazine A ISSN 0141–8610 print/ISSN 1460-6992 online
http://www.tandf.co.uk/journals

single crystals of NiAl along the cube axes (also known as the 'hard' orientation), $\langle 010 \rangle$ slip is suppressed, since there is no resolved shear stress on the $a\langle 010 \rangle$ dislocations. Instead, slip occurs through $a\langle 111 \rangle$ dislocations at lower temperatures (Loretto and Wasilewski 1971, Pascoe and Newey 1971, Sun *et al.* 1995). Deformation by this mode requires much higher yield and flow stresses, compared with soft (non-$\langle 001 \rangle$-oriented) NiAl.

Starting at intermediate temperatures in hard-oriented NiAl, there is a sharp decrease in the yield strength with increasing temperature. This coincides with a change in deformation mode from $a\langle 111 \rangle$ to non-$a\langle 111 \rangle$ processes (Fraser *et al.* 1973b, Kim 1990, Field *et al.* 1991, Kim and Gibala 1991). There has been considerable debate in the literature regarding the activity of $a\langle 010 \rangle$ versus $a\langle 101 \rangle$ dislocations beyond this slip transition temperature (Fraser *et al.* 1973a, Kim 1990). Interestingly, deformation by $a\langle 010 \rangle$ dislocations has been reported to occur primarily in stoichiometric NiAl (Fraser *et al.* 1973a), while extensive $a\langle 101 \rangle$ slip has been observed in slightly Ni-rich Ni–Al (Kim 1990). The apparent difference in deformation mode has been explained in brief elsewhere (Mills *et al.* 1998b, Srinivasan *et al.* 1998).

Despite the vast amount of research performed on the deformation processes in NiAl, there is relatively little understanding of the exact mechanism and details of the slip transition in hard-oriented single crystals. One reason for the lack of information concerning the dislocation mechanisms associated with the slip transition is that geometrical kinking of compression samples tends to occur just below the slip transition temperature. The profusion of $a\langle 010 \rangle$ activity, which is generated by kinking, therefore obscures the underlying processes involving $a\langle 111 \rangle$ dislocations. Earlier *in-situ* hot-stage studies on Ni–48 at.% Al (Kim and Gibala 1991), however, have provided valuable information about the mechanism of decomposition of $a\langle 111 \rangle$ dislocations at elevated temperatures.

In this paper, we attempt to provide, mainly through experimental observations, the sequence of events by which the slip transition occurs at intermediate temperatures in Ni–44 at.% Al. This alloy composition is particularly interesting for this purpose since the tendency for kinking is significantly reduced relative to the stoichiometric composition. Consequently, we have been able to observe deformation microstructures in Ni–44 at.% Al (at temperatures below the slip transition temperature) that are not a result of kinking. The theoretical basis behind the process of slip transition has been discussed in detail in the accompanying paper (Brown *et al.* 2000), and elsewhere (Srinivasan *et al.* 1998). Deformation beyond the slip transition temperature in Ni–44 at.% Al has also been addressed elsewhere (Mills *et al.* 1998b).

§ 2. Experimental

Single crystals of Ni–44 at.% Al were grown by a Bridgman technique at General Electric Aircraft Engines (Cincinnati, Ohio) and homogenized in an Ar atmosphere for 50 h at 1589 K. [001]-oriented compression specimens approximately 4 mm in diameter and 8 mm in length were machined from the ingots. A length : diameter ratio of 2 : 1 is helpful in reducing the tendency for kinking (Field *et al* 1991). Compression tests were performed on an Instron testing apparatus, at various temperatures and to various strain levels at strain rates between 10^{-4} and $10^{-5}\,s^{-1}$. The compression tests were conducted at Glenn Research Center, National Aeronautics and Space Administration (NASA), and at The Ohio State University. All samples were cooled rapidly by forced air immediately following unloading.

Discs for transmission electron microscopy (TEM) were cut from deformed samples using a low-speed saw. Final preparation of thin foils for TEM study consisted of jet polishing using a Struers twin-jet electropolisher. A current of 25–30 mA and a voltage of 4–8 V was used in the polishing process. TEM investigations were carried out on a Philips CM 200 (LaB_6 cathode) operating at 200 kV. For anisotropic elasticity image simulations, the image software CUFOUR developed by R. Schaublin and P. Stadelmann was used. Atomistic simulations, discussed in the accompanying paper (Brown *et al.* 2000), were performed using the embedded-atom method (EAM) theory, previously developed by Daw and Baskes (1984).

§ 3. Results and discussion

3.1. *Deformation at low temperatures (300–500 K)*

Figure 1 shows the variation of yield strength versus temperature for Ni–44 at.% Al. The data are for a strain rate of $1.4 \times 10^{-4}\,s^{-1}$. Detailed TEM analysis has been performed on samples deformed in the temperature range 300–1050 K. Samples deformed at temperatures for which TEM results are discussed in this paper are indicated by the open squares in the figure. The slip transition (which is also associated with a sharp decrease in yield strength at intermediate temperatures) is observed to occur around 800 K for Ni–44 at.% Al. The region of sharp decrease in yield strength will be termed the 'knee' in the yield strength curve. The slip transition in stoichiometric NiAl is associated with the onset of appreciable tensile ductility, and a large increase in the strain-rate sensitivity (Field *et al.* 1991). Note the remarkably athermal nature of the yield strength data below the temperature T_k of the 'knee', and the sharp dependence of yield strength on temperature above T_k.

At very low temperatures (77–298 K), ⟨111⟩{112} slip dominates in Ni–50 at.% Al (Sun *et al.* 1995), and reverts to ⟨111⟩{110} slip at higher temperatures.

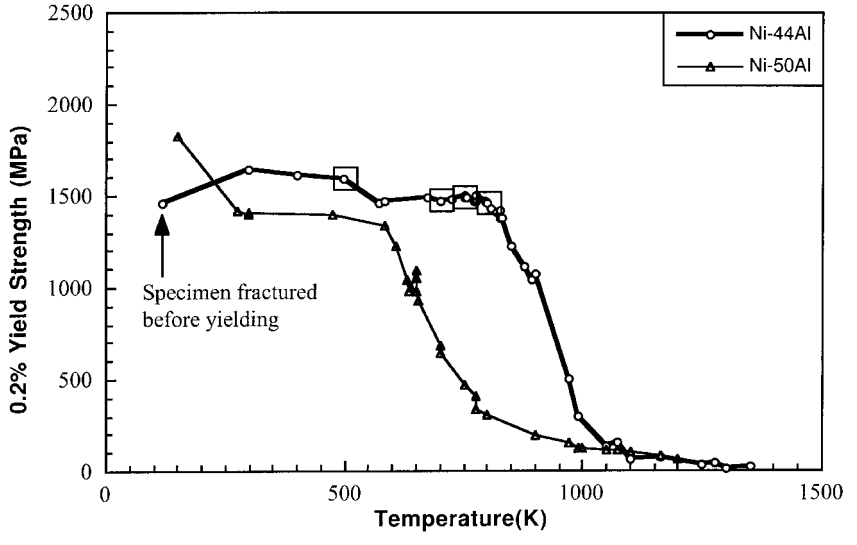

Figure 1. Graph of yield strength versus temperature for Ni–44 at.% Al and Ni–50 at.% Al. The slip transition in both alloys is associated with a sharp drop in yield strength, termed as the 'knee' in the yield strength curve. The 'knee' for Ni–44 at.% Al occurs at a higher temperature than for Ni–50 at.% Al.

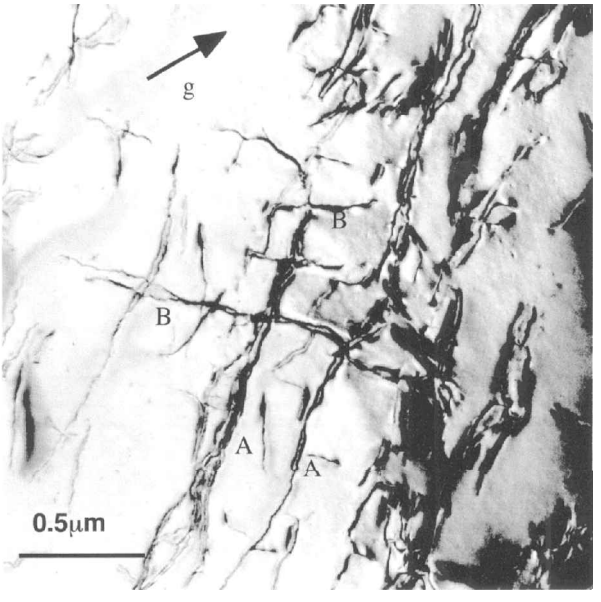

Figure 2. $\mathbf{g} = (020)$ bright-field micrograph in Ni–44 at.% Al showing $a\langle 111\rangle$ dislocations in the dislocation microstructure for Ni–44 at.% Al deformed 1.2% at 500 K. The beam direction is close to [001]. The dislocations are elongated near the edge orientation and are wavy in nature, owing to the extensive cross-slip. Dislocations A are $a[111]$ dislocations, and B are $a[1\bar{1}1]$ dislocations.

The microstructure in Ni–44 at.% Al deformed at 500 K (strain rate, $1.4 \times 10^{-4}\,s^{-1}$) is characterized by long wavy edge $a\langle 111\rangle$ dislocations, as shown in figure 2. This is indicative of extensive cross-slip of screw dislocations between the {110} and the {112} planes (the existence of both slip modes has been verified by line trace analysis). The edge components are much longer than their screw counterparts, possibly implying that the edges have the lowest mobility in this deformation regime. The dipole-like configuration seen for many of the edge segments (in figure 2) indicates that these edge components may be present following the cross-slip and annihilation of screw components of the dislocations. It should be noted here that the edge dipoles are very narrow (less than 0.05 μm), making it difficult to determine whether they lie on the same plane or are separated out of their glide plane. Consequently, it is not possible to determine conclusively whether the large density of near-edge component is due to the relatively low mobility of edge segments, or to the cross-slip annihilation of screw segments. However, earlier studies on stoichiometric NiAl have indicated that the edge dipoles are probably created owing to cross-slip and annihilation of screw segments (Noebe *et al.* 1995, Sun *et al.* 1995), rather than through the extension of screw components of an $a\langle 111\rangle$ loop.

At higher temperatures in Ni–44 at.% Al (between approximately 600 and 800 K), $a\langle 111\rangle$ slip occurs exclusively on {110} planes. Detailed TEM investigations carried out between 700 and 800 K have revealed interesting microstructural details associated with the $a\langle 111\rangle$ dislocations and provide a more complete picture of the slip transition than has been determined previously. As mentioned earlier, the slip transition in Ni–44 at.% Al occurs around 800 K and is achieved through decomposition of $a\langle 111\rangle$ dislocations. The subsequent sections describe this decomposition

process. It should be mentioned again that this Ni-rich composition offers a unique opportunity to study this decomposition process, as the stoichiometric composition is prone to extensive geometrical kinking just below the 'knee' temperature.

3.2. *Dislocation configurations associated with the slip transition*

Earlier studies (Field *et al.* 1991, Kim and Gibala 1991, Srinivasan *et al.* 1997) have indicated that the slip transition is achieved through the decomposition of $a\langle 111\rangle$ dislocations, as follows:

$$a[111] \rightarrow a[101] + a[010]. \tag{1}$$

This reaction is energetically favourable near the edge orientation for the $a[111]$ dislocation on the $(\bar{1}01)$ glide plane (Fu and Yoo 1992). While the driving force for the decomposition reaction may be ascribed to this energy consideration, there is no obvious way to explain the thermal activation which appears to be required for this reaction to proceed to completion. Thus, it is not clear why stable glide of $a\langle 111\rangle$ dislocations on $\{101\}$ planes is commonly observed at lower temperatures (Loretto and Wasilewski 1971, Veyssière and Noebe 1992, Sun *et al.* 1995, Srinivasan *et al.* 1996), rather than the occurrence of spontaneous decomposition.

Figure 3 shows the deformation microstructure in Ni–44 at.% Al deformed 0.7% at 750 K (strain rate, $1.4 \times 10^{-4}\,s^{-1}$). Deformation occurs through $a\langle 111\rangle\{110\}$ slip. As seen at lower temperatures, the dislocations are again largely of near-edge character. However, the dislocations tend not to be in dipole configurations (as in figure 2) but, instead, are often seen as individual $a\langle 111\rangle$ dislocations. The observation of elongated loops of $a\langle 111\rangle$ dislocations with a majority of edge character indicates that the edge segments are indeed the more slowly moving components of the dislocation.

There are several distinctive dislocation configurations seen in figure 3 which are not observed at lower temperatures. The first are the small $a[111]$ loops indicated for example at L in the figure. Second are the loop-like features seen at A in the figure.

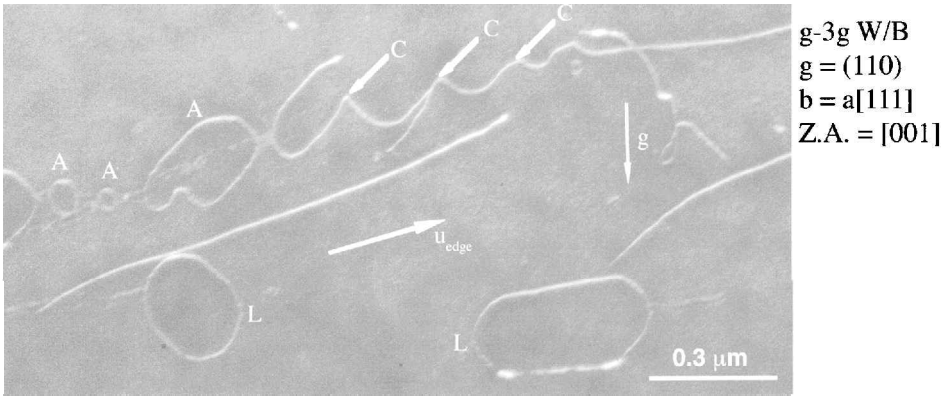

Figure 3. Weak-beam (**g**−3**g**) **g** = (110) image in Ni–44 at.% Al deformed 0.7% at 750 K. $a[111]$ dislocations are dominant in the microstructure. The zone axis is near [001]. The line direction of the edge-oriented $a[111]$ dislocations is indicated as $\mathbf{u}_{edge}$. The arrows indicate cusp-like features (labelled C) observed on several of the $a[111]$ dislocations. Several loops of $a[111]$ dislocations are also observed (labelled L). In addition, other loop-like features (discussed in the text) are indicated as A.

These are, however, not complete $a[111]$ loops, as will be discussed below. Another distinction compared with the structures at lower temperatures is the presence of sharp cusp-like features on many of the near-edge segments, which are labelled C in the figure. The remainder of the $a\langle 111\rangle$ segments appear to bow around these cusp-like features, resulting in the formation of a near-screw $a\langle 111\rangle$ line length around the cusp. The cusps appear to be local pinning points on the near-edge segment.

Figure 4 shows a higher-magnification view of the $a\langle 111\rangle$ dislocations discussed above. The $a[\bar{1}\bar{1}1]$ half-loops (shown in the figure) seem to be linked by $a[001]$

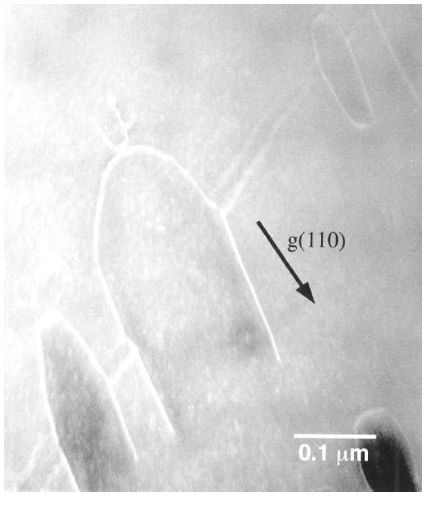

(*a*)

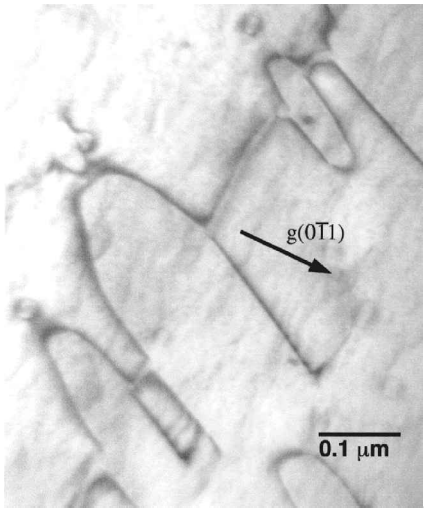

(*b*)

Figure 4. (*a*) $\mathbf{g} = (110)$ weak-beam $\mathbf{g}-3\mathbf{g}$ (zone axis between [001] and $[\bar{1}11]$); (*b*) $\mathbf{g} = (0\bar{1}1)$ bright-field (zone axis near [011]) micrographs showing the nature of $a[001]$ linking dipole-like segments between $a[\bar{1}\bar{1}1]$ half-loops observed in Ni–44 at.% Al strained 0.7% at 750 K. Note that the $a[001]$ dislocations are observed in residual contrast in (*a*). The strain rate is $1.4 \times 10^{-4}\,s^{-1}$.

dislocations. These dislocations are observed in residual contrast for a **g**-(110) diffracting vector. Diffraction contrast and tilting experiments have shown these linking dislocations to be a[001] dipoles aligned along the [110] directions. It is possible that the screw component of the $a[\bar{1}\bar{1}1]$ dislocations can cross-slip from a (101) plane to a (112) plane and subsequently decompose along the edge orientation as follows:

$$a[\bar{1}\bar{1}1] \rightarrow a[\bar{1}\bar{1}0] + a[001]. \tag{2}$$

The $a[\bar{1}\bar{1}0]$ segments can subsequently annihilate, leaving a[001] dipoles in the microstructure. However, this explanation is incomplete and cannot explain why the a[001] dipoles also cannot annihilate. Also, it is hard to explain why the $a[\bar{1}\bar{1}0]$ dislocations should in fact move and annihilate on the (112) plane, since they cannot glide on that plane. Thus, no satisfactory explanation can be provided at this juncture for the observation of the a[001] dipoles, but the logical explanation for their presence seems to be related to the cross-slip of the $a[\bar{1}\bar{1}1]$ dislocations on to other {112} (or {110}) planes in the $[\bar{1}\bar{1}1]$ zone.

We now turn attention to the cusped configurations identified earlier in figure 3. Figure 5 shows a magnified view of an $a[\bar{1}11]$ dislocation, in Ni–44 at.% Al deformed 0.4% at 800 K (a slightly higher temperature than for figure 3, note that $T_k = 800$ K for Ni–44 at.% Al). The overall alignment of the dislocations is still near the edge orientation (actually aligned approximately along both ⟨111⟩ directions in the glide plane). However, local deviations from this overall alignment are seen all along the dislocation, such that the local line length is actually predominantly near the screw orientation. Particularly interesting are the short segments that are of near-edge orientation (70.5° away from the screw orientation). While the screw line lengths appear to be compact, the near-edge component has decomposed into a[101] and a[010] dislocations, as indicated in the figure. Note that the temperature of deformation, where the first observable signs of decomposition of a⟨111⟩ dislocations occur, is very close to T_k in Ni–44 at.% Al.

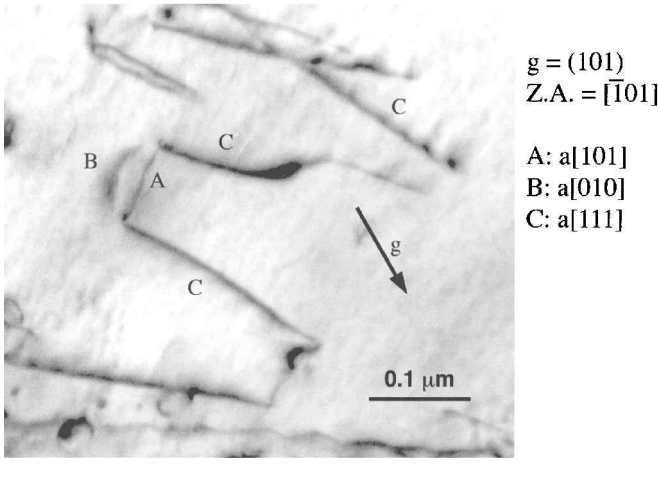

Figure 5. Higher-magnification **g** = (101) image showing the local decomposition of an a[111] dislocation occurring along the 70°, $[1\bar{1}1]$ direction on the $(\bar{1}01)$ glide plane: zone axis near $[\bar{1}01]$. The screw-oriented portions of the segment are undecomposed. Decomposition is energetically favoured near the edge orientation.

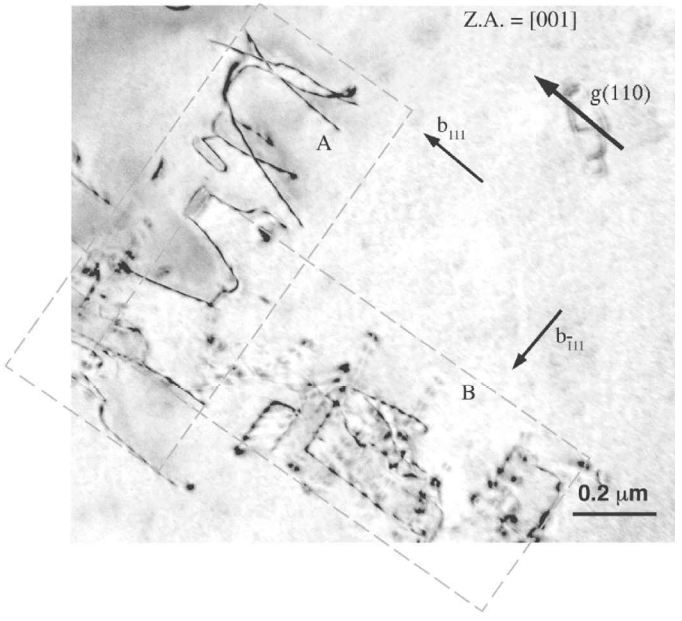

Figure 6. Deformation microstructure in Ni–44 at.% Al strained 0.4% at 800 K at $1.4 \times 10^{-4}\,s^{-1}$: zone axis [001]. Two different slip systems are shown. The slip system in region A shows $a[111](\bar{1}01)$ activity. The slip system in region B shows $a[011]$ and $a[\bar{1}00]$ dislocations, and some $a[\bar{1}11]$ dislocations that are still undecomposed. These dislocations have a $(0\bar{1}1)$ glide plane.

The same Ni–44 at.% Al sample deformed 0.4% at 800 K actually shows slip activity on two separate systems. While the dislocations from the one dominant $a\langle 111\rangle\{110\}$ slip system (shown in figure 5 and region A of figure 6) appear to be in the process of decomposing, the other slip system consists mainly of $a\langle 101\rangle$ and $a\langle 010\rangle$ dislocations that would add up to $a\langle 111\rangle$ dislocations on the same glide plane, indicating that complete decomposition of the $a\langle 111\rangle$ dislocations has occurred. Region B of figure 6 shows an example of this decomposed microstructure.

At higher strains at 800 K, TEM investigation reveals that complete decomposition of $a\langle 111\rangle$ dislocations has occurred, resulting in $a\langle 011\rangle$ and $a\langle 100\rangle$ dislocations in the microstructure. The $a\langle 100\rangle$ dislocations are frequently observed in dipole configurations, and all dislocations are consistently aligned along $\langle 111\rangle$ directions. Figure 7, which shows the deformation microstructure in Ni–44 at.% Al strained 1.7% at 800 K (which is very close to the 'knee' temperature in Ni–44 at.% Al) is representative of this microstructure. The observation of the $a\langle 100\rangle$ dipoles in figure 7 cannot be easily explained through a simple decomposition process of the $a\langle 111\rangle$ dislocations (a simple decomposition along the 70°, $\langle 111\rangle$ directions would result in a parallel arrangement of $a\langle 100\rangle$ and $a\langle 011\rangle$ dislocations). Also, it is interesting to note that several $a\langle 011\rangle$ and $a\langle 100\rangle$ dislocations are observed in pairs, as indicated by the letter p, shown in figure 7. These paired dislocations would add up to $a\langle 111\rangle$ dislocations on the same glide plane†. This is further evidence that decomposition of

†Using the fact that the line direction of all the dislocations is $\langle 111\rangle$, and the trace formed by the intersection of these pairs of $a\langle 011\rangle$ and $a\langle 100\rangle$ dislocations is $\langle 100\rangle$, it can be determined that they lie on a single $\{011\}$ plane.

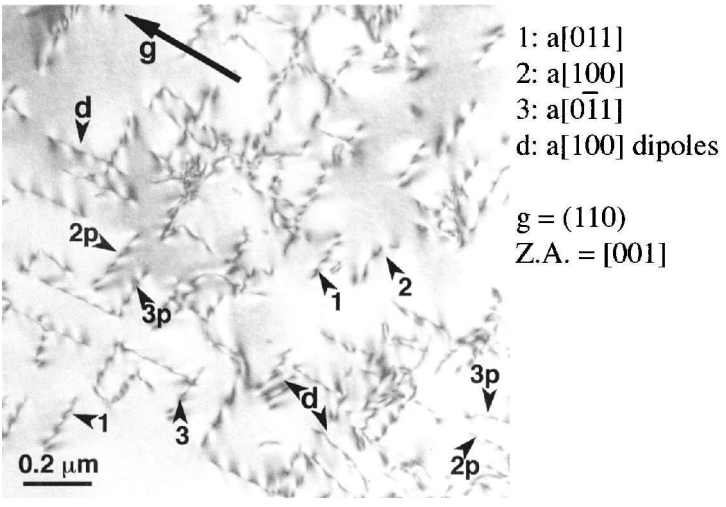

Figure 7. Deformation microstructure in Ni–44 at.% Al strained 1.7% at 800 K. The diffracting vector is (110), and the zone axis (Z.A.) is close to [001]. Only $a\langle 011\rangle$and $a\langle 100\rangle$ dislocations are observed in the microstructure. The $a\langle 011\rangle$ and $a\langle 100\rangle$ dislocations that are indicated by the letter p (denoting pairs) add up to $a\langle 111\rangle$ dislocations on the same glide plane, indicating that decomposition of $a\langle 111\rangle$ dislocations is probably responsible for the observed deformation microstructure. Note the observation of a[100] dipoles indicated by d. All dislocations are observed along ⟨111⟩ directions.

$a\langle 111\rangle$ dislocations indeed occurs, leading to the slip transition. For completeness, we shall mention here that the average separation between the $a\langle 010\rangle$ dipole segments is approximately 0.05 μm. This information is important to validate the results obtained through anisotropic elasticity calculations that are discussed in the accompanying paper (Brown *et al.* 2000). Note the flag-like contrast observed on the dislocations in figure 7. This contrast is fully consistent with that observed through image simulations using the CUFOUR program.

Earlier anisotropic elastic calculations (Fu and Yoo 1992) have shown that it is indeed energetically favourable for $a\langle 111\rangle$ dislocations to undergo a glide decomposition reaction near the edge orientation. The reaction is favoured for approximately 55–125° from the screw orientation and is elastically unfavourable for all other orientations. The decomposition force is a maximum along the 70.5°, ⟨111⟩ direction in the glide plane (Fu and Yoo 1992, Brown *et al.* 2000). This can explain the alignment of dislocations along the near-edge ⟨111⟩ directions, but the calculations by Fu and Yoo (1992) do not provide an understanding of the temperature dependence of the decomposition reaction and hence do not explain the observed microstructure in NiAl satisfactorily. The results of atomistic and elasticity calculations, discussed in the accompanying paper (Brown *et al.* 2000), reveal additional details regarding the nature of the decomposition process of the $a\langle 111\rangle$ dislocations.

3.3. *Effect of strain rate*

Compression tests were performed at lower strain rates to determine the effect of changes in strain rate on the deformation microstructure and macroscopic properties of Ni–44 at.% Al at temperatures at and below T_k. The strain rate has very little effect on the yield strength at temperatures below T_k. Ni–44 at.% Al samples

deformed below the 'knee', at strain rates of 10^{-4} and $10^{-5}\,s^{-1}$ show very similar yield strengths and flow behaviour between 700 and 775 K. However, above T_k, the yield strength is a very strong function of the strain rate, for both Ni–50 at.% Al (Pascoe and Newey 1971) and Ni–44 at.% Al (R. Srinivasan and M. J. Mills 1999, unpublished research). (Note that, since we have limited the scope of discussion in this paper to deformation at and below the 'knee', the issue of strain-rate sensitivity above the 'knee' will be discussed elsewhere.) The value of T_k itself does seem to be somewhat affected by changes in the strain rate. The microstructure of an Ni–44 at.% Al sample deformed 1.6% at 750 K, at a lower strain rate of $1.4 \times 10^{-5}\,s^{-1}$, consists primarily of screw $a\langle 111\rangle$ segments (with very little non-screw line length) and is very similar to that observed in figure 5 (Ni–44 at.% Al, deformed at 800 K and $1.4 \times 10^{-5}\,s^{-1}$). In general, decreasing the strain rate by an order of magnitude seems to decrease T_k by approximately 25–50 K, based on experimental observations. An explanation for the observed behaviour will be provided, through a model of the $a\langle 111\rangle$ decomposition in the accompanying paper (Brown *et al.* 2000).

3.4. *The role of $a\langle 101\rangle$ dislocation mobility in the slip transition process*

We now turn attention to the mobility of $a\langle 101\rangle$ dislocations. During the decomposition process, there is no macroscopic resolved shear stress (or climb force) on the $a\langle 010\rangle$ decomposition product, but there is resolved shear stress on the $a\langle 101\rangle$ dislocation. Studies beyond the slip transition temperature in Ni–48 at.% Al (Kim and Gibala 1991), Ni–44 at.% Al (Srinivasan *et al.* 1997) and stoichiometric NiAl bicrystals (Miracle 1991 Mills *et al.* 1998a) have demonstrated the existence of $a\langle 101\rangle\{101\}$ glide, at least in a finite-temperature window immediately beyond T_k in the respective compounds. This raises two important points.

(*a*) Why does $a\langle 111\rangle$ motion dominate over $a\langle 101\rangle$ motion below T_k?
(*b*) What role does the motion of $a\langle 101\rangle$ dislocations have to play in the process of decomposition and slip transition?

A partial answer to question (*a*) is provided below, limiting the discussion to the scope of this paper.

Estimates of the Peierls' stress for $a[\bar{1}01]$ dislocations aligned along the $[\bar{1}\bar{1}1]$ direction, based on EAM calculations, indicate that the $a[\bar{1}01]$ dislocation has a much higher friction stress at lower temperatures than $a[\bar{1}11]$ dislocations do (M. S. Daw, J. Brown, R. Srinivasan and M. J. Mills 1999, unpublished research). Deformation at lower temperatures is consequently dominated by $a\langle 111\rangle$ glide. The lower mobility of $a\langle 101\rangle$ dislocations persists up to T_k. The accompanying paper, which presents the model for $a\langle 111\rangle$ decomposition, discusses in detail the importance of $a\langle 101\rangle$ dislocation mobility in determining the micromechanics of the $a\langle 111\rangle$ decomposition process. It is important to note that, at temperatures significantly greater than T_k (e.g. $T = 875$ K), deformation has been observed to occur only through $a\langle 101\rangle\{101\}$ glide in Ni–44 at.% Al (R. Srinivasan and M. J. Mills 1999, unpublished research).

Since we have mentioned the $a\langle 101\rangle$ mobility as a critical factor in determining the decomposition reaction, it is essential to determine whether the nucleation or the mobility of $a\langle 101\rangle$ dislocations is the critical step in determining $a\langle 101\rangle$ activity (or the lack of it) at temperatures near and below T_k. It is possible that the motion of $a\langle 101\rangle$ dislocations is dependent on nucleation of these dislocations, and not so

much on the critical resolved shear stress for $a\langle 101\rangle$ glide (which is an indication of the mobility of $a\langle 101\rangle$ dislocations). A temperature-change test was conducted to help to clarify this question. A Ni–44 at.% Al sample was deformed in two stages: firstly, 1.9% strain at 875 K (strain rate, $2 \times 10^{-5}\,s^{-1}$), followed by, secondly, 0.96% at 700 K (strain rate, $2 \times 10^{-5}\,s^{-1}$). As discussed in other pertinent literature (Srinivasan *et al*. 1997, R. Srinivasan and M. J. Mills, 1999, unpublished research), the temperature of 875 K was chosen as the optimum temperature for $a\langle 101\rangle$ activity (and subsequent decomposition of $a\langle 101\rangle$ dislocations). Figure 8 (*a*) shows the stress–strain plot for the previously described test while figure 8 (*b*) shows the deformation microstructure for the sample after this sequence of deformation. At point A in figure 8 (*a*) (after deformation at 875 K, completion of stage I), $a\langle 101\rangle$ dislocations would be present in the deformation microstructure, as confirmed through monotonic tests at that temperature and strain rate; no $a\langle 111\rangle$ activity has been observed in these monotonic tests (R. Srinivasan and M. J. Mills, 1999, unpublished research). After the second stage of deformation (point B in figure 8 (*a*), completion of stage II), both $a\langle 111\rangle$ and $a\langle 101\rangle$ dislocations (as well as $a\langle 010\rangle$ decomposition products†) are observed in the final deformation microstructure, as shown in figure 8 (*b*). However, the yield strength obtained from the second stage of deformation is essentially the same as that for an undeformed sample at 700 K. This result suggests that, even though the pre-injected $a\langle 101\rangle$ dislocations are plentiful, they are no longer mobile below T_k. Therefore, $a\langle 111\rangle$ dislocations have to be generated, as observed in figure 8 (*b*), in order to accommodate plastic deformation at 700 K. These experiments directly indicate that $a\langle 101\rangle$ mobility is indeed strongly temperature dependent.

As will be evident from the decomposition model presented in the accompanying paper (Brown *et al*. 2000), if the $a\langle 101\rangle$ dislocation mobility is lower than the $a\langle 111\rangle$ mobility, there can be no expansion of the decomposition node, as has been experimentally observed (see figure 5). Evolution of the decomposition node leading to complete decomposition of the $a\langle 111\rangle$ dislocations has been discussed in detail in the accompanying paper (Brown *et al*. 2000).

Decomposition of $a\langle 111\rangle$ dislocations and slip transition are thus closely related. The important feature linking both these processes is $a\langle 101\rangle$ dislocation mobility, which is strongly temperature dependent (R. Srinivasan and M. J. Mills 1999, unpublished research). The results of the temperature-change test (figures 8 (*a*) and (*b*)) also illustrate the strong temperature dependence of the $a\langle 101\rangle$ dislocation mobility. Miracle (1991) and Mills and Miracle (1993) have also addressed the issue of the temperature-dependent critical resolved shear stress for $a\langle 101\rangle$ dislocations, but no clear link had been established previously between this proposition and the actual mechanism of slip transition.

§ 4. Unresolved issues

The detailed study of the deformation microstructure presented above has attempted to show that decomposition of $a\langle 111\rangle$ dislocations does indeed lead to

† The presence of $a[010]$ and $a[001]$ dislocations in this microstructure deserves additional comment. As indicated in previous studies on bicrystals of NiAl (Mills and Miracle 1993, Mills *et al*. 1998a), decomposition of $a\langle 011\rangle$ dislocations is energetically favoured along the edge orientation. The observation of $a[010]$ and $a[001]$ dislocations along the edge orientations is thus fully consistent with the operation of $a[011](0\bar{1}1)$ glide, and subsequent decomposition of $a[011]$ dislocations along the edge orientation.

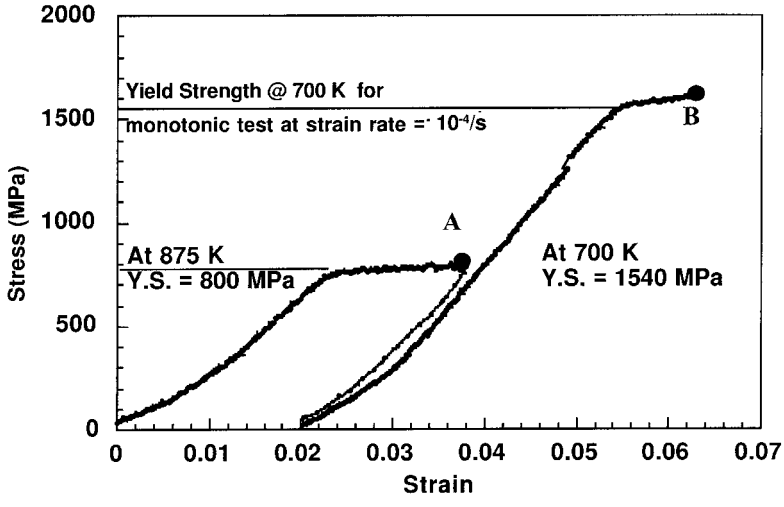

(*a*)

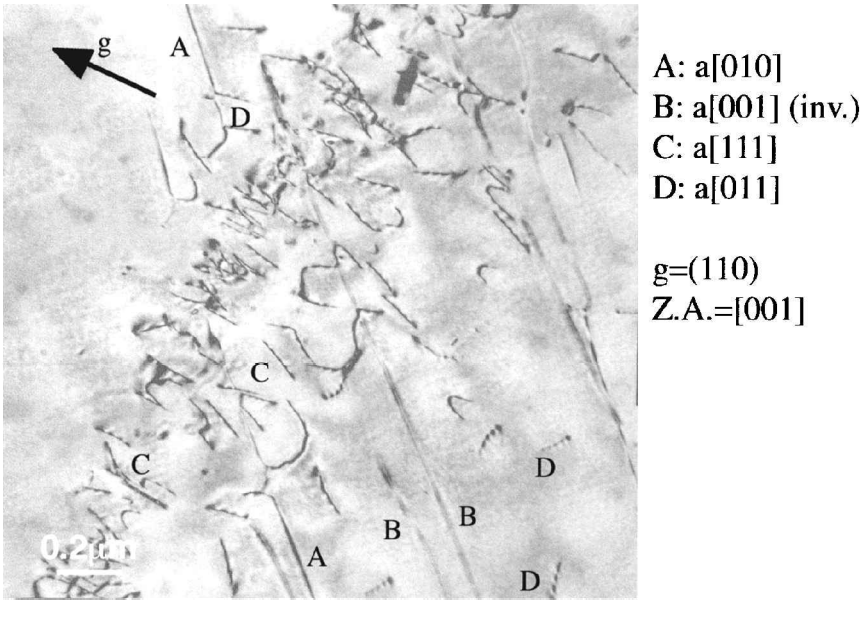

(*b*)

Figure 8. (*a*) Stress-strain graph for a two-stage deformation experiment performed on Ni–44 at.% Al to test the temperature dependence of mobility of $a\langle 101\rangle$ dislocations. At 875 K, $a\langle 101\rangle$ dislocations (and $a\langle 010\rangle$ dislocations formed through decomposition of $a\langle 101\rangle$ dislocations) were injected into the microstructure. The specimen was then cooled to 700 K and deformed in the $a\langle 111\rangle$ deformation regime. The presence of $a\langle 101\rangle$ sources does not seem to affect the deformation behaviour, as seen in (*b*). $a\langle 111\rangle$ dislocations are generated at 700 K, since the $a\langle 101\rangle$ sources are immobile at this temperature. The yield strength (Y.S.) at 700 K is also unaffected by the presence of $a\langle 101\rangle$ dislocations. (*b*) Micrograph showing $a[011]$ dislocations generated at 875 K (labelled D), $a[010]$ and $a[001]$ dislocations generated through decomposition of $a[011]$ dislocations (labelled A and B respectively), and $a[111]$ dislocations generated at 700 K. The $a[001]$ dislocations are observed in residual contrast: zone axis near [001].

the slip transition in Ni–44 at.% Al. However, there are two outstanding questions that the experimental evidence has raised.

(*a*) Anisotropic elasticity calculations (Fu and Yoo 1992, Brown *et al.* 2000) show that decomposition is favoured near the edge orientation for Ni–50 at.% Al and Ni–44 at.% Al, irrespective of temperature, but stable $a\langle 111\rangle$ activity is observed in Ni–44 at.% Al up to 800 K, as discussed above in the text. What is the reason for the stability of $a\langle 111\rangle$ dislocations in Ni–44 at.% Al (in general, for Ni-rich compositions, and possibly for Ni–50 at.% Al) at temperatures below the 'knee'?

(*b*) Figure 7 shows several interesting features associated with the post-decomposition microstructure, such as the observation of $a\langle 010\rangle$ dipoles. The $a\langle 010\rangle$ dipoles are very commonly observed and are clearly an important by-product of the $a\langle 111\rangle$ decomposition process. Simple elasticity theory, which predicts a straightforward decomposition (e.g. an $a[\bar{1}\bar{1}1]$ dislocation decomposing into $a[\bar{1}01]$ and $a[0\bar{1}0]$ dislocations along the $[\bar{1}11]$ direction on the (101) glide plane), cannot easily account for the observation of $a[010]$ dipoles in the deformation microstructure. What is the reason for the observed post-decomposition microstructure at temperatures at (and just above) the 'knee'?

Explanations for these outstanding issues are presented in the theoretical study and analysis of the $a\langle 111\rangle$ decomposition process discussed in the accompanying paper (Brown *et al.* 2000), which culminates in a model for $a\langle 111\rangle$ decomposition based on the microstructural observations presented above.

§ 5. Conclusions

Microstructural evidence has shown the progression of decomposition of $a\langle 111\rangle$ dislocations in Ni–44 at.% Al. Decomposition occurs along near-edge $\langle 111\rangle$ orientations in the glide plane. The decomposition force on the $a\langle 111\rangle$ dislocation is highest along the near-edge (70.5° from the screw orientation) $\langle 111\rangle$ directions in the glide plane. Several interesting features are associated with the decomposition reaction, such as the formation of locally decomposed nodes on $a\langle 111\rangle$ segments, and the observation of $a\langle 010\rangle$ dipoles along with $a\langle 101\rangle$ dislocations in the post-decomposition microstructure. The slip transition in Ni–44 at.% Al is a direct result of the decomposition of $a\langle 111\rangle$ dislocations.

Acknowledgements

Support for this project was provided by the US Department of Energy under grant DE-FG02-96ER45550 (for M.J.M. and R.S.), and by the National Science Foundation (for M.S.D. and J.B.). R.S. would like to acknowledge the help of Dr T. Neeraj in conducting some of the mechanical tests.

References

Brown, J., Srinivasan, R., Mills, M. J., and Daw, M. S., 2000, *Phil. Mag.* A, **80**, 2855.
Darolia, R., Lahrman, D., and Field, R., 1992, *Scripta metall.*, **26**, 1007.
Daw, M. S., and Baskes, M. I., 1984, *Phys. Rev.* B, **29**, 6443.
Field, R. D., Lahrman, D. F., and Darolia, R., 1991, *Acta metall. mater.*, **39**, 2951.
Fraser, H. L., Loretto, M. H., and Smallman, R. E., 1973a, *Phil. Mag.* A, **28**, 667.
Fraser, H. L., Smallman, R. E., and Loretto, M. H., 1973b, *Phil. Mag.* A, **28**, 651.
Fu, C. L., and Yoo, M. H., 1992, *Acta metall. mater.*, **40**, 703.

KIM, J. T., 1990, PhD Thesis, University of Michigan.
KIM, J. T., and GIBALA, R., 1991, *High Temperature Ordered Intermetallic Alloys IV,* Materials Research Society Symposium Proceedings, Vol. 213, edited by L. A. Johnson, D. P. Pope and J. O. Stiegler (Pittsburgh, Pennsylvania: Materials Research Society), p. 261.
LEVIT, V. I., BUL, I. A., HAL, J., and KAUFMAN, M. J., 1996, *Scripta mater.,* **34**, 1925.
LORETTO, M. H., and WASILEWSKI, R. J., 1971, *Phil. Mag.,* **23**, 1311.
MILLS, M. J., and MIRACLE, D. B., 1993, *Acta metall. mater.,* **41**, 85.
MILLS, M. J., SRINIVASAN, R., and DAW, M. S., 1998a, *Phil. Mag.* A, **77**, 801.
MILLS, M. J., SRINIVASAN, R., SAVAGE, R. D., NOEBE, and DAW, M. S., 1998b, *Interstitial and Substitutional Solute Effects in Intermetallics,* edited by I. Baker, R. D. Noebe and E. P. George (Warrendale, Pennsylvania: Metallurgical Society of AIME), p. 99.
MIRACLE, D. B., 1991, *Acta metall. mater.,* **39**, 1457.
NOEBE, R. D., BOWMAN, R. R., and NATHAL, M. V., 1995, *Physical Metallurgy and Processing of Intermetallic Compounds,* edited by N. S. Stoloff and V. K. Sikka (London: Chapman & Hall), p. 212.
NOEBE, R. D., and GARG, A., 1995, Technical Memorandum NASA TM 106981, National Aeronautics and Space Administration.
PASCOE, R. T., and NEWEY, C. W. A., 1971, *Metal. Sci. J.,* **5**, 50.
SRINIVASAN, R., SAVAGE, M. F., DAW, M. S., NOEBE, R. D., GARG, A., and MILLS, M. J., 1997, *Structural Intermetallics II,* edited by M. V. Nathal, R. Darolia and C. T. Liu (Warrendale, Pennsylvania: Metallurgical Society of AIME), p. 662.
SRINIVASAN, R., SAVAGE, M. F., DAW, M. S., NOEBE, R. D.,MILLS, M. J., 1998, *Scripta mater.,* **39**, 457.
SRINIVASAN, R., SAVAGE, M. F., MILLS, M. J., DAW, M. S., and NOEBE, R. D., 1996, *Deformation, Fatigue and Fracture of Ordered Intermetallic Materials,* edited by W. O. Soboyejo, T. S. Srivatsan and H. L. Fraser (Warrendale, Pennsylvania: Metallurgical Society of AIME), p. 325.
SUN, Y. Q., TAYLOR, G., DAROLIA, R., and HAZZLEDINE, P. M., 1995, *High Temperature Ordered Intermetallic Alloys VI,* Materials Research Society Symposium Proceedings, Vol. 364, edited by J. Horton *et al.* (Pittsburgh, Pennsylvania: Materials research Society), p. 261.
VEYSSIÈRE, P., and NOEBE, R. D., 1992, *Phil. Mag.* A, **65**, 1.